

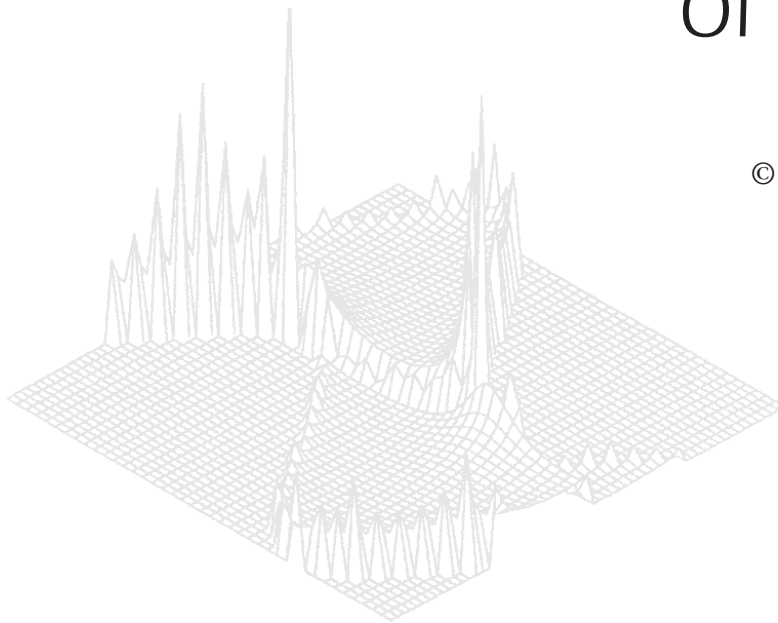
---

**C S I R O   P U B L I S H I N G**

---

# Australian Journal of Physics

Volume 52, 1999  
© CSIRO Australia 1999



A journal for the publication of  
original research in all branches of physics

**[www.publish.csiro.au/journals/ajp](http://www.publish.csiro.au/journals/ajp)**

All enquiries and manuscripts should be directed to

*Australian Journal of Physics*

**CSIRO PUBLISHING**

PO Box 1139 (150 Oxford St)

Collingwood

Vic. 3066

Australia

Telephone: 61 3 9662 7626

Facsimile: 61 3 9662 7611

Email: [peter.robertson@publish.csiro.au](mailto:peter.robertson@publish.csiro.au)



Published by **CSIRO PUBLISHING**  
for CSIRO Australia and  
the Australian Academy of Science



## Effect of Radial Wavevector on Collisional Drift Waves in a Toroidal Helic

*J. L. V. Lewandowski<sup>A</sup> and R. M. Ellem*

Department of Theoretical Physics, RSPHysSE,  
Australian National University,  
Canberra, ACT 0200, Australia.

<sup>A</sup> Also at the Plasma Research Laboratory, RSPHysSE, ANU.

### *Abstract*

A 3-field model for collisional drift waves, in the ballooning representation, for a low-pressure stellarator plasma is presented. In particular, the effect of a finite radial mode number ( $\equiv \theta_k$ ) is studied, and the linear growth rates for the fluctuating plasma density, electrostatic potential and electron temperature are computed numerically by solving the 3-field model as an initial-value problem. Numerical results for a 3-field period stellarator with low global magnetic shear are then presented. It is found that, in a system with small global magnetic shear, the case  $\theta_k = 0$  yields the fastest linear growth rate.

### 1. Introduction

Magnetically confined plasmas are intrinsically nonuniform in space. Spatial gradients in the plasma density and (ion and electron) temperatures typically generate slow, short-scale, collective phenomena known as drift waves (Horton 1989). These drift waves, along with other microinstabilities (Liewer 1985; Tang 1978), are believed to be responsible for the large cross-field transport, the so-called ‘anomalous transport’ (Rosenbluth and Sagdeev 1984; Manheimer and Lashmore-Davies 1989), which is observed in tokamaks and stellarators.

Electrostatic drift wave turbulence can be excited by various mechanisms. Some destabilising mechanisms for drift waves in low- $\beta$  plasmas can be provided by collisions, Landau resonances, trapped particle effects (Rosenbluth and Sagdeev 1984; Manheimer and Lashmore-Davies 1989), ionisation effects (Ware *et al.* 1992) and finite parallel (Marchand and Guzdar 1982) and perpendicular (Tang and Luhmann 1976) currents. In general, the magnetic shear is the dominant stabilising mechanism. For example, the standard tokamak configuration, typically has a strong, positive global magnetic shear. However, some stellarator configurations, such as W7-AS (Grieger *et al.* 1985), TJ-2 (Alejaldre *et al.* 1990) and H1-NF (Hamberger *et al.* 1990), have a small, or even negligible, global magnetic shear. In these configurations, the local properties of the magnetic shear can play an important role, as recently suggested by Waltz and Boozer (1993). In order to gain a better understanding of stellarator cross-field transport, it is crucial to access the importance of the confining magnetic field key attributes (such as the local magnetic shear and the normal curvature) on drift wave dynamics. This paper is part of an ongoing project concerned with drift waves in three-dimensional geometries, such as stellarators and tokamaks with field coil ripples (Persson *et*

*al.* 1996; Persson and Lewandowski 1997; Lewandowski 1997*a*, 1997*b*, 1997*c*, 1998).

In this paper, we use the ballooning representation to study a 3-field model for collisional drift waves, in the linear regime which is valid for low- $\beta$  stellarator plasmas. Here, we have included the effect of radial mode number ( $\theta_k$ ), which was neglected in a 3-field (Lewandowski 1997*a*) and a 4-field (Lewandowski 1997*b*) model for resistive drift-type modes. In a system with low-global magnetic shear, such as H1-NF, it can be argued that the dependence of the fastest linear growth rate on  $\theta_k$  must be weak. Extensive numerical simulations for *ideal* MHD ballooning modes show that the  $\theta_k$  dependence is indeed weak, and one can argue that the slow  $\theta_k$  dependence must, *a priori*, also be valid for *resistive* modes. In this case, one can assume that  $\theta_k = 0$  in all calculations (Lewandowski 1997*a*). However, it has not yet been *proven* (either analytically or numerically) that the  $\theta_k$  dependence of linear resistive modes in a low-shear system is indeed weak. The aim of this paper is to numerically study the  $\theta_k$  dependence of such modes for a realistic stellarator plasma.

The paper is organised as follows; in Section 2, the equilibrium magnetic field is specified in straight-field-line (Boozer) coordinates; in Section 3, a fluid model, valid for arbitrary 3-dimensional geometry, is presented and the ballooning representation, including the effect of a finite radial mode number, is discussed (analytical calculations of the geometrical effects are reported in Appendix B). The numerical results are presented and discussed in Section 4. We conclude with some remarks in Section 5.

## 2. The Equilibrium

For 3-dimensional equilibria, the equilibrium magnetic field is conveniently written in straight-field-line (Boozer) coordinates (Boozer 1980, 1981, 1982)

$$\mathbf{B} = \nabla\alpha \times \nabla\psi, \quad (1)$$

where  $\alpha \equiv \zeta - q(\psi)\theta$  is the field line label and  $2\pi\psi$  is the enclosed poloidal flux. The variables  $\theta$  and  $\zeta$  are, respectively, the poloidal and toroidal angle-like coordinates (with period  $2\pi$ ). For a stellarator geometry, it is customary to use  $s \equiv \Psi/\Psi_b$  as a radial label, where  $\Psi$  is the enclosed toroidal flux and  $\Psi_b$  is the enclosed toroidal flux evaluated at the plasma boundary. By construction, the (normalised) radial label ranges from 0 (at the magnetic axis) to 1 (at the last closed magnetic surface). The confining magnetic field then reads  $\mathbf{B} = \dot{\psi}\nabla\alpha \times \nabla s$ , where a dot denotes a derivative with respect to  $s$ . In the coordinate system  $(s, \theta, \zeta)$ , the Jacobian of the transformation  $\mathcal{J} \equiv [\nabla s \cdot (\nabla\theta \times \nabla\zeta)]^{-1}$  has the dimensionality of a volume. In a stellarator geometry, this equilibrium is computed numerically using the ideal magnetohydrodynamic (MHD) equations (as described in Appendix A).

## 3. The Model (General Geometry)

We consider a low-temperature, high-density plasma in which, for simplicity, the ions are assumed to be cold ( $\tau \equiv T_i/T_e \ll 1$ ). For modes with perpendicular wavelength much larger than the ion thermal gyro-radius and parallel wavelength much larger than the electron mean free path, the plasma is in the collisional

regime and Braginskii's (1965) fluid equations can be used to describe the drift wave dynamics. We consider slow, drift-type modes satisfying

$$\frac{\omega}{\omega_{ci}} \ll 1 \text{ and } \frac{k_{\parallel}}{k_{\perp}} \ll 1. \quad (2)$$

Here  $k_{\parallel}$  and  $k_{\perp}$  are the typical magnitude of the parallel and perpendicular wavevectors, respectively,  $\omega \sim \partial/\partial t$  is the typical mode frequency and  $\omega_{ci} \equiv eB/m_i c$  is the ion cyclotron frequency. For perturbations with parallel phase velocity much larger than the ion thermal velocity,  $\omega/k_{\parallel} \gg v_{thi}$ , the ion parallel motion can be neglected. The inclusion of ion parallel motion has been shown to provide a stabilising mechanism for the drift waves. For wavelengths much larger than the Debye length, the plasma is quasineutral.

The basic equations (Braginskii 1965) are the ion continuity equation,

$$\frac{\partial n}{\partial t} + \nabla \cdot (n\mathbf{v}_i) = 0, \quad (3)$$

the ion momentum balance equation,

$$m_i n \left( \frac{\partial}{\partial t} + \mathbf{v}_i \cdot \nabla \right) \mathbf{v}_i = en \left( \mathbf{E} + \frac{\mathbf{v}_i \times \mathbf{B}}{c} \right) - \mathbf{R}_{ei}, \quad (4)$$

the electron momentum equation (neglecting electron inertia and viscous effects)

$$\nabla p_e + en \left( \mathbf{E} + \frac{\mathbf{v}_e \times \mathbf{B}}{c} \right) - \mathbf{R}_{ei} = 0, \quad (5)$$

the quasineutrality condition,

$$\nabla \cdot \mathbf{J} = 0, \quad (6)$$

and the electron energy equation

$$\frac{3}{2} n \left( \frac{\partial}{\partial t} + \mathbf{v}_e \cdot \nabla \right) T_e = -nT_e \nabla \cdot \mathbf{v}_e - \nabla \cdot \mathbf{q}_e + \frac{\mathbf{J} \cdot \mathbf{R}_{ei}}{en}, \quad (7)$$

where the electron viscosity and the ion–electron equilibration term ( $\sim m_e/m_i \ll 1$ ) have been neglected. In equations (4), (5) and (7),  $\mathbf{R}_{ei}$  is the momentum transfer to the electrons due to collisions with ions. In the ion momentum equation (4), the ion collisional viscosity has been neglected. The ion collisional viscosity has a stabilising influence on the drift wave (Coppi *et al.* 1967). For slow cross-field motions satisfying (2), the perpendicular components of the ion and electron velocities can be obtained perturbatively. This derivation is standard, and hence, we only state the results (Lewandowski 1997a) that

$$\mathbf{v}_{i\perp} = \mathbf{v}_E + \mathbf{v}_{pi} + \mathbf{v}_{coll} \quad (8)$$

is the cross-field ion velocity, obtained from equation (4), and

$$\mathbf{v}_{e\perp} = \mathbf{v}_E + \mathbf{v}_{de} + \mathbf{v}_{coll} \quad (9)$$

is the perpendicular electron velocity obtained from Ohm's law (5). In equations (8) and (9)

$$\begin{aligned} \mathbf{v}_E &\equiv \frac{c}{B} \mathbf{E} \times \hat{\mathbf{e}}_{\parallel}, \\ \mathbf{v}_{pi} &\equiv \omega_{ci}^{-1} \hat{\mathbf{e}}_{\parallel} \times \left( \frac{\partial}{\partial t} + \mathbf{v}_E \cdot \nabla \right) \mathbf{v}_E, \\ \mathbf{v}_{coll} &\equiv \frac{c}{enB} \hat{\mathbf{e}}_{\parallel} \times \mathbf{R}_{ei}, \\ \mathbf{v}_{de} &\equiv \frac{c}{enB} \nabla p_e \times \hat{\mathbf{e}}_{\parallel} \end{aligned} \quad (10)$$

are the lowest order  $\mathbf{E} \times \mathbf{B}$  drift velocity, the ion polarisation drift velocity, the ion–electron–collision-driven drift velocity and the electron diamagnetic drift velocity, respectively. Here,  $\hat{\mathbf{e}}_{\parallel} \equiv \mathbf{B}/B$  is a unit vector parallel to the equilibrium magnetic field. The parallel component of the electron momentum equation (5) provides the parallel current density (assuming  $v_{i\parallel} = 0$ ) which is then substituted into the charge neutrality equation

$$\nabla \cdot \mathbf{J}_{\parallel} = -\nabla \cdot \mathbf{J}_{\perp}, \quad (11)$$

where the perpendicular current density  $\mathbf{J}_{\perp} = en(\mathbf{v}_{pi} - \mathbf{v}_{de})$  is obtained by subtracting equation (9) from equation (8). After linearisation of equation (11), we neglect the (small) parallel equilibrium current density  $J_{\parallel 0}$ ; this approximation is justified in medium-size stellarators such as the toroidal heliac H1-NF. A non-zero  $J_{\parallel 0}$  implies that a relatively strong electric field exists (possibly generated locally by the heating system) which, in turn, suggests a strong departures from thermodynamic equilibrium. In the present paper, such strong departures from thermodynamic equilibrium are not taken into account. Introducing the normalised plasma density perturbation  $\tilde{n} \equiv \delta n/n_0$ , the normalised electrostatic potential  $\tilde{\Phi} \equiv e\Phi/T_{e0}$  (where  $T_{e0}$  is the equilibrium electron temperature) and the normalised fluctuating electron temperature  $\tilde{T}_e = \delta T_e/T_{e0}$ , we note that  $v_E \sim v_{de} \gg v_{pi} \gg v_{coll} \sim v_E/\xi_e$ , where  $\xi_e \equiv \omega_{ce}\tau_e$  is a dimensionless quantity related to the plasma collisionality. Here  $\omega_{ce}$  is the electron cyclotron frequency and  $\tau_e$  is the electron basic collisional time as calculated by Braginskii (1965). For a high-density, low-temperature, magnetised plasma (typically  $B \sim 1$  T,  $n \sim 10^{12}$  cm $^{-3}$ ,  $T_e \sim 25$  eV), we have  $\xi_e \sim 10^5 \gg 1$ , showing that the collision-driven drift velocity is much smaller than the  $\mathbf{E} \times \mathbf{B}$ -drift velocity.

For modes with short perpendicular wavelength (but still long enough so that  $k_{\perp}\rho_{thi} \ll 1$ , where  $\rho_{thi}$  is the ion thermal gyro-radius) and long parallel wavelength, one can use the ballooning representation for fluctuating quantities (Antonsen and Lane 1980):

$$\tilde{\Phi} \equiv \frac{e\Phi}{T_{e0}} = \hat{\Phi}(x_{\parallel}, t) \exp\left(i\frac{S}{\epsilon}\right), \quad (12)$$

where  $S$  is the eikonal,  $x_{\parallel}$  is the length along the magnetic field line,  $\hat{\epsilon} \ll 1$  is a smallness parameter (expansion parameter) and  $\hat{\Phi}$  is the amplitude. If  $L$  denotes the typical equilibrium scalelength, we assume that the amplitude  $\hat{\Phi}$  and the eikonal  $S$  are slowly-varying functions of space; more specifically, we assume that  $|L\hat{\Phi}^{-1}\nabla\hat{\Phi}| \sim |LS^{-1}\nabla S| = \mathcal{O}(1)$ . Following Antonsen and Lane (1980), we also demand that the eikonal satisfies  $\mathbf{B} \cdot \nabla S = 0$ . From the Clebsch representation (1), it is clear that  $S = S(\alpha, \psi)$ . Since the safety factor is a flux surface quantity,  $q = q(\psi)$ , one can use  $q$  as a radial coordinate. Then we get (to leading order)

$$\begin{aligned} \nabla\tilde{\Phi} &= i\hat{\epsilon}^{-1}\nabla S \tilde{\Phi} \\ &= i\hat{\epsilon}^{-1}\frac{\partial S}{\partial\alpha}(\nabla\alpha + \theta_k\nabla q)\tilde{\Phi}, \end{aligned} \quad (13)$$

where  $\theta_k \equiv (\partial S/\partial q)/(\partial S/\partial\alpha)$  is the so-called radial mode number. Making the usual assumption that the eikonal has the form  $S = \alpha + \bar{S}(q, \alpha)$  with  $|\partial\bar{S}/\partial\alpha| \ll 1$ , equation (13) then yields  $\nabla\tilde{\Phi} = i\mathbf{k}_{\perp}\tilde{\Phi} + \mathcal{O}(\tilde{\Phi}/L)$  where

$$\mathbf{k}_{\perp} \equiv n(\nabla\alpha + \theta_k\hat{q}\nabla s), \quad (14)$$

and  $n \equiv 1/\hat{\epsilon} \gg 1$  is the (large) toroidal mode number. In a previous paper (Lewandowski 1997a), collisional drift waves in stellarator geometry were studied for the case  $\theta_k = 0$ . Strictly speaking, the parameter  $\theta_k$  must be varied until the fastest growing mode is found. We note that  $\theta_k \neq 0$  modifies the *radial* (along  $\nabla s$ ) component of the lowest-order perpendicular wavevector. As it turns out, all the secular terms in the final eigenmode equations are modified for  $\theta_k \neq 0$ . As for the time scales involved in the problem, the equilibrium plasma density is assumed to vary on the transport timescale,  $\omega_{ci}^{-1} \partial n_0/\partial t/n_0 = \mathcal{O}(\epsilon^3) \ll \omega_{ci}^{-1} \partial\hat{n}/\partial t/\hat{n} = \mathcal{O}(\epsilon)$ , where  $\epsilon \sim \omega/\omega_{ci} \ll 1$  is a smallness parameter. A similar eikonal representation (12) is assumed for the perturbed density and electron temperature.

Our model equations, written in normalised form, have been derived elsewhere (Lewandowski 1997a). After linearisation, these are: the ion continuity equation

$$\frac{\partial\hat{n}}{\partial t''} = i(S_{\perp 1} - S_{\perp 2})\hat{\Phi}, \quad (15)$$

the quasineutrality condition

$$\frac{\partial\hat{\Phi}}{\partial t''} = \mathcal{L} [iS_{\perp 1}(\hat{n} + \hat{T}_e) - \xi_c (L_n^2\nabla_{\parallel}^2\hat{F} - L_n Q_{\parallel}\nabla_{\parallel}\hat{F})], \quad (16)$$

and the electron energy equation

$$\begin{aligned} \frac{\partial\hat{T}_e}{\partial t''} &= \xi_c [L_n^2\nabla_{\parallel}^2\hat{G} - Q_{\parallel}L_n\nabla_{\parallel}\hat{G}] \\ &+ i\hat{\Phi} \left(\frac{2}{3}S_{\perp 1} - \eta_e S_{\perp 2}\right) + i\hat{n} \left(\frac{2}{3}S_{\perp 2} - \frac{2}{3}S_{\perp 1}\right) + i\hat{T}_e \left(\frac{2}{3}S_{\perp 2} - \frac{7}{3}S_{\perp 1}\right). \end{aligned} \quad (17)$$

In equations (15)–(17),  $\mathbf{Q} \equiv L_n \nabla B / B$  is a dimensionless quantity proportional to the curvature of the magnetic field line;  $L_n \equiv \bar{a} (dn_0/ds/n_0)^{-1}$  is the radial density scalelength ( $\bar{a}$  is the average minor radius of the last closed magnetic surface);  $\omega_* e \equiv (cT_{e0} k_\theta) / e B_0 L_n$  is the electron diamagnetic frequency ( $k_\theta \equiv m q / \bar{a}$ );  $\mathcal{L} \equiv (B_* / \xi_\perp k_\theta \rho_{s0})^2$  is related to the polarisation drift term;  $B_* \equiv B / B_0$  is the magnetic field strength normalised to  $B_0$  (magnetic axis);  $\xi_\perp \equiv \sqrt{\hat{\mathbf{e}}_\perp \cdot \hat{\mathbf{e}}_\perp}$ ;  $\hat{\mathbf{e}}_\perp \equiv \mathbf{k}_\perp / k_\theta$  is the normalised perpendicular wavevector;  $\xi_c \equiv \omega_{ce0} \tau_e / k_\theta L_n \gg 1$  is a nondimensional quantity arising for the parallel electron conductivity; and, finally,  $\omega_{ce0}$  is the electron cyclotron frequency evaluated at the magnetic axis. In equation (11), we have defined  $\hat{F} \equiv 2(1 + \mu_1) \hat{T}_e + 2\hat{h}$ , where  $\mu_1 = 0.71$  is a thermoelectric coefficient in the electron–ion momentum transfer  $\mathbf{R}_{ei}$ , and  $\hat{h} = \hat{n} - \hat{\Phi}$  is the non-adiabatic response of the electrons. In the electron energy equation (16),  $\hat{G} \equiv 2[2(1 + \mu_1)^2 + \mu_2] \hat{T}_e / 3 + 4(1 + \mu_1) \hat{h} / 3$  and  $\mu_2 = 3.2$  is a thermoelectric coefficient in the parallel electron heat conductivity. The geometrical effects enter through  $\mathcal{L}$  (polarisation drift),  $B_*$  (magnetic field strength),  $\xi_\perp$  (norm of the perpendicular wavevector) as well as the curvature term

$$S_{\perp 1} \equiv \frac{2}{B_*} (\hat{\mathbf{e}}_\parallel \times \hat{\mathbf{e}}_\perp) \cdot \mathbf{Q}, \quad (18)$$

and the diamagnetic term

$$S_{\perp 2} \equiv \frac{\bar{a} \sqrt{g^{ss}}}{B_*} [\hat{\mathbf{e}}_\perp \cdot (\hat{\mathbf{e}}_\parallel \times \hat{\mathbf{n}})], \quad (19)$$

where  $g^{ss} = \nabla s \cdot \nabla s$  is a metric element,  $\hat{\mathbf{e}}_\parallel \equiv \mathbf{B} / B$  is the unit vector along  $\mathbf{B}$  and  $\hat{\mathbf{n}} \equiv \nabla s / (\nabla s \cdot \nabla s)^{1/2}$  is a unit vector normal to the magnetic surface and pointing outwards. Finally, we would like to point out that the term  $Q_\parallel$  in equations (16) and (17) is related to the compression of the unit vector  $\hat{\mathbf{e}}_\parallel$  (Lewandowski 1997a). In stellarator geometry, the *extended* toroidal angle  $\zeta$  can be used as a label along the magnetic field line, so that we write  $x_\parallel = x_\parallel(\zeta)$  in the amplitude (12).

Equations (15) and (17) form a system of three time-dependent, coupled partial differential equations to be solved along the magnetic field line. The amplitudes  $\hat{\Phi}$ ,  $\hat{n}$  and  $\hat{T}_e$  are assumed to vanish for large values of the extended poloidal angle since, for any physical solution, the eigenfunctions must be square integrable:

$$\int_{-\infty}^{+\infty} |\hat{\Phi}(\zeta', t)|^2 d\zeta' < \infty. \quad (20)$$

In the next section, we present the numerical solution of equations (15)–(17) in a stellarator geometry.

#### 4. Numerical Results

The system of equations (15)–(17) has been solved numerically as an initial-value problem along the field line. In view of the fast parallel electron heat transport, explicit methods require a very small time step of integration. Furthermore the perpendicular transport in the electron temperature equation (16) involves a term of the form

$$\frac{\partial \widehat{T}_e}{\partial t''} = C_{\perp} \widehat{T}_e + \dots, \quad (21)$$

which is found to be numerically unstable even for a very small time step of integration. Therefore the diffusive terms in (16) and (17) have been treated implicitly with centred differences along the extended toroidal angle. The terms  $\partial \widehat{\Phi} / \partial t''$  and  $\partial \widehat{T}_e / \partial t''$  have also been treated implicitly. However, the ion continuity equation (15) has been explicitly treated in full detail. The system of equations reduces to a tridiagonal form which can be easily solved using the elimination method (Press *et al.* 1983); this method is easy to implement and suitable for highly-vectorised numerical codes. Other numerical details have been reported elsewhere (Lewandowski 1997*a*, 1997*b*).

The growth rate for the perturbed electrostatic potential has been computed as follows:

$$\gamma_{\Phi}(t'') = \frac{1}{\langle |\widehat{\Phi}| \rangle} \frac{\partial \langle |\widehat{\Phi}| \rangle}{\partial t''}, \quad (22)$$

where  $|F| \equiv (FF^*)^{\frac{1}{2}}$  denotes the magnitude of  $F$  and  $\langle G \rangle$  denotes an average over the extended toroidal angle,

$$\langle G \rangle \equiv \frac{1}{2\zeta_m} \int_{\zeta_0 - \zeta_m}^{\zeta_0 + \zeta_m} G(\zeta') d\zeta', \quad (23)$$

where  $\zeta_0$  is a poloidal angle of reference and  $\zeta_m$  is a free parameter. Perturbed quantities are assumed to vanish at  $\zeta_0 \pm \zeta_m$ . Note that this is consistent with the square-integrability condition (19). The parameter  $\zeta_m$  must be chosen sufficiently large so that the growth rate (21) and the mode extent along the field line become independent of  $\zeta_m$ . The growth rates for the perturbed density  $\tilde{n}$ , and the fluctuating electron temperature  $\tilde{T}_e$ , assume a similar form to equation (22).

As shown in Appendix B, the inclusion of a nonzero radial mode number  $\theta_k$  in the geometrical quantities leads to the appearance of new secular terms. The details of the calculations for  $\nabla_{\parallel}$ ,  $\xi_{\perp}$ ,  $S_{\perp 1}$  and  $S_{\perp 2}$  are also presented in Appendix B. To verify that the new geometrical effects were included correctly, we have run a typical case with  $\theta_k = 0$ , and then compared the results with previously known results (Lewandowski 1997*a*, 1997*b*).

Because of the rapid variation of the equilibrium quantities along the magnetic field line (see Figs 4–6 in Lewandowski 1997*a*), we must use a small mesh size along the extended toroidal angle; for the simulations discussed below, we have used  $\Delta\zeta = \pi/200$ . A smaller mesh size does not modify the eigenfunctions or the eigenvalues (growth rates); however, the time step must be drastically reduced [typically, the critical time step consistent with *numerical* stability scales like  $1/(\Delta\zeta)^2$ ]. We have chosen a normalised time step of  $\Delta t'' = \omega_{*e} \Delta t = 10^{-4}$ . The parameter  $\zeta_m$  must be chosen so that the final (physical) growth rate is independent of the actual value of  $\zeta_m$ . However, if  $\zeta_m$  is too large, then the numerical solution of our model equations becomes prohibitive. To estimate  $\zeta_m$ , we note that the secular terms will ultimately govern the extent of the modes along the field line. The secular terms enter through combinations of the multiple-valued vector  $\nabla\alpha$ , that is

$$\nabla\alpha = \nabla\zeta - q\nabla\theta - \dot{q}\theta\nabla s. \quad (24)$$

Clearly the secular part of  $|\nabla\alpha|$  arises from the last term on the right-hand side of equation (23). If we take  $\alpha_0 = 0$  as the field line of reference, we note that for  $|\zeta| \geq \zeta_c \equiv |q/\dot{q}|$  the secular last term on the right-hand side of equation (23) dominates over the other two terms. For the numerical calculations discussed below, we have chosen the  $s_0 = 0.9$  magnetic surface, where  $q(s_0) = 0.9$  and  $\dot{q}(s_0) = -0.1$  (i.e. a small negative global magnetic shear). Then we expect the secular terms in the model equations to dominate for  $|\zeta| \geq 10$ . The eigenfunctions for  $\tilde{n}$ ,  $\tilde{\Phi}$  and  $\tilde{T}_e$  are typically localised within  $|\zeta| \leq 12$ , which agrees reasonably well with the estimate above (see Figs 7–9 in Lewandowski 1997*a*). To ensure proper convergence, we have chosen  $\zeta_m = 40$ , which is a few times the magnitude of  $\zeta_c$ . A longer integration distance does not modify the results for the eigenfunctions or the eigenvalues.

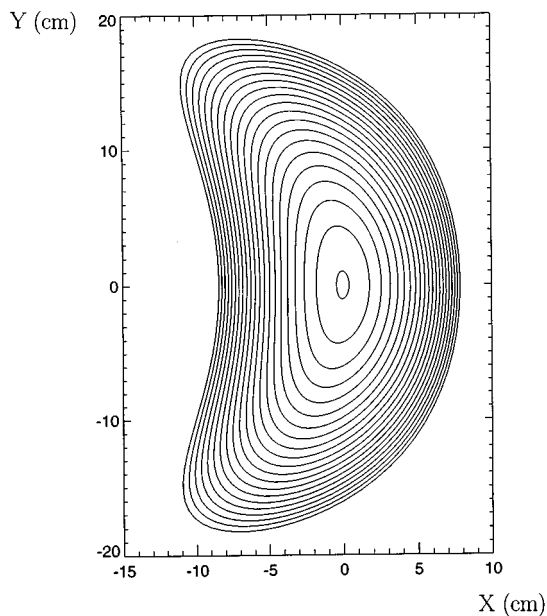


**Fig. 1.** Poloidal cross section of the H1-NF plasma at the plane  $\phi = 0$ . A (reduced) set of 21 nested magnetic surfaces is shown. The full equilibrium has been calculated with 100 magnetic surfaces equally spaced in the radial coordinate  $s$ . The position of the symmetry point  $\theta_0 = \zeta_0 = 0$  used in the numerical calculations corresponds to  $X = 7.6$  cm and  $Y = 0$  cm.

Fig. 1 shows a poloidal cross section, at the plane  $\phi = 0$ , for the standard configuration of H1-NF. For the sake of clarity, only a reduced set of 21 nested magnetic surfaces is shown in Fig. 1. The full equilibrium was determined using a set of 100 magnetic surfaces. We note the characteristic ‘bean shape’ of the magnetic surface cross sections of H1-NF. The magnetic axis is located at  $x = y = 0$ .

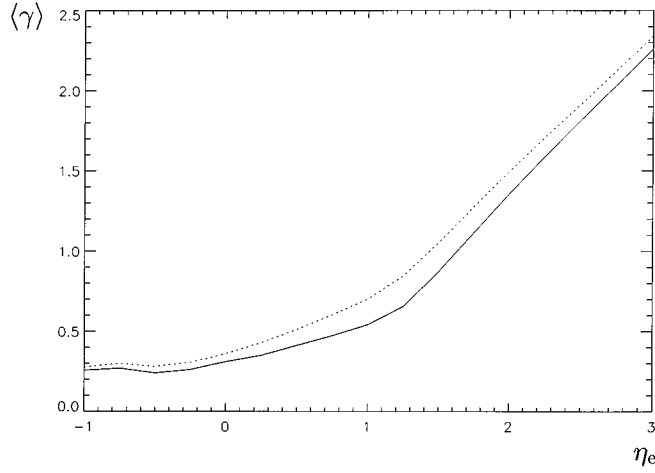


**Fig. 2.** Average linear growth rate  $\langle \gamma \rangle$  at the end of the simulations as a function of the electron temperature gradient parameter  $\eta_e \equiv d \ln T_{e0} / d \ln n_0$ , where  $n_0$  is the equilibrium plasma density and  $T_{e0}$  is the equilibrium electron temperature. The dotted line corresponds to the case  $\theta_k = 0$ ; the solid line is for  $\theta_k = \pi/2$ . Other parameters used in the simulations are  $T_e = 25$  eV,  $n_0 = 5 \times 10^{12}$  cm $^{-3}$ ,  $L_n = 3.5$  cm and  $b = (k_\theta \rho_{s0})^2 = 0.5$ .

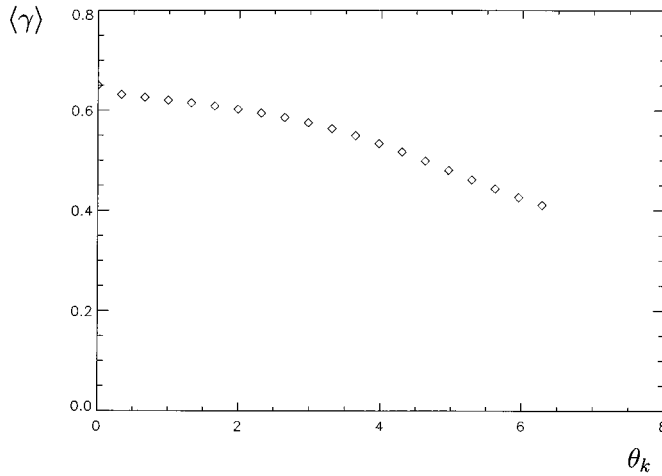


**Fig. 3.** Average linear growth rate  $\langle \gamma \rangle$  at the end of simulations as a function of the radial mode number. The temperature gradient parameter is  $\eta_e = 1.0$ ; other parameters are the same as in Fig. 2.

Fig. 2 shows the average growth rate  $\langle \gamma \rangle \equiv (\gamma_\Phi + \gamma_n + \gamma_{T_e})/3$  at the end of the simulations, as a function of the electron temperature gradient parameter. Other parameters are  $T_e = 25$  eV,  $n_0 = 5 \times 10^{12}$  cm $^{-3}$ ,  $L_n = 3.5$  cm and  $b = (k_\theta \rho_s)^2 = 0.5$ . For all of the results presented below a vectorisation of 95% to 98% was achieved. Each point (i.e. the growth rate) in Figs 2 and 3 requires

260 minutes of central-processor-unit (CPU) time on a Supercomputer VPP300 (Utsumi *et al.* 1994). The dotted line shows the case  $\theta_k = 0$ , whereas the solid line corresponds to the case  $\theta_k = \pi/2$ . We note that the average growth rate for  $\theta_k \neq 0$  is smaller than  $\langle \gamma \rangle$  for *all* values of the electron temperature gradient parameter.

Fig. 3 shows the average growth rate  $\langle \gamma \rangle$  as a function of the radial mode number. The electron temperature gradient parameter is  $\eta_e = 1.0$ ; all other parameters are the same as in Fig. 2. As can be seen in this figure, the fastest growth rate occurs at  $\theta_k = 0$ . Interestingly, for *ideal* MHD ballooning modes and for the same magnetic configuration as in Figs 1-3, the fastest linear growth rate is also found for  $\theta_k = 0$  (Cuthbert 1999).

## 5. Conclusion

We have studied resistive drift-type modes in the linear regime and for the low- $\beta$  edge plasma of a stellarator. An eikonal representation was used for the fluctuating quantities, in which the radial mode number  $\theta_k$  was taken into account. The set of equations has been solved as an initial-value problem along the magnetic field line.

It has been shown that a nonzero  $\theta_k$  is responsible for additional secular terms in the model equations, and in particular, in the curvature term and the lowest-order perpendicular wavevector.

In general, the fastest linear growth rate must be optimised with respect to the parameter  $\theta_k$ . We have found that  $\theta_k = 0$  corresponds to the fastest linear growth. For the toroidal heliac H-1NF, the same trend for *ideal* MHD ballooning modes was recently observed by Cuthbert (1999). However, when the global magnetic shear is large, the largest growth rate does *not* necessarily occur at  $\theta_k = 0$  (Cuthbert *et al.* 1998).

Therefore, for a stellarator plasma with low global magnetic shear, both ideal and resistive drift-type ( $k_{\parallel}/k_{\perp}$ ) modes have their fastest growth rates for  $\theta_k = 0$ . We believe that this is an important conclusion: since the fastest growth rate occurs at a vanishing radial mode number, a scan in the parameter  $\theta_k$  is not necessary. This greatly speeds up the numerical solution of the time-dependent problem.

What is not understood, however, is why the ideal *and* non-ideal (resistive) modes with  $k_{\parallel}/k_{\perp} \ll 1$  have their fastest linear growth rate at  $\theta_k = 0$  in a plasma with low global magnetic shear. We believe that a better understanding of the geometrical effects in the ballooning representation would be desirable.

## Acknowledgments

One of us (J.L.V.L.) would like to thank Professor R. Singh for fruitful discussions. J.L.V.L. was supported by a Natural Sciences and Engineering Research Council of Canada (NSERC) Research Fellowship.

## References

- Alejaldre, C., Gozalo, J. J. A., Perez, J. B., Magana, F. C., Diaz, J. R. C., Perez, J. G., Lopez-Fraguas, A., Garcia, L., Krivienski, V. I., Martin, R., Navarro, A. P., Perea, A., Rodriguez-Yunta, A., Ayza, M. S., and Varias, A. (1990). *Fusion Tech.* **17**, 131.  
 Antonsen, T. M., and Lane, J. B. (1980). *Phys. Fluids* **23**, 1205.

- Boozer, A. H. (1980). *Phys. Fluids* **23**, 904.
- Boozer, A. H. (1981). *Phys. Fluids* **24**, 1999.
- Boozer, A. H. (1982). *Phys. Fluids* **25**, 520.
- Braginskii, S. I. (1965). ‘Review of Plasma Physics’ (Consultants Bureau: New York).
- Coppi, B., Hendel, H. W., Perkins, F., and Politzer, P. A. (1967). Proc. Conf. on the Physics of Quiescent Plasmas, Frascati, Italy, Vol. 1 (Associazione Euratom-CNEN: Rome).
- Cuthbert, P. (1999). Ballooning eigenmode structure of low-shear stellarators. (to be submitted).
- Cuthbert, P., Lewandowski, J. L. V., Persson, M., Singleton, D. B., Dewar, R. L., Nakajima, N., and Cooper, W. A. (1998). *Phys. Plasmas* **5**, 2921.
- D’haeseleer, W. D., Hitchon, W. N. G., Callen, J. D., and Shohet, J. L. (1983). ‘Flux Coordinates and Magnetic Field Structure’ (Springer: Berlin).
- Grieger, G., Renner, H., and Wobig, H. (1985). *Nucl. Fusion* **25**, 1231.
- Hamberger, S. M., Blackwell, B. D., Sharp, L. E., and Shenton, D. B. (1990). *Fusion Tech.* **17**, 123.
- Hendel, H. W., Chu, T. K., and Politzer, P. A. (1968). *Phys. Fluids* **11**, 2426.
- Hirshman, S. P., and Meier, H. K. (1985). *Phys. Fluids* **28**, 1387.
- Hirshman, S. P., and Whitson, J. C. (1983). *Phys. Fluids* **26**, 3553.
- Horton, W. (1989). *Phys. Fluids B* **1**, 524.
- Lewandowski, J. L. V. (1997a). *Phys. Plasmas* **4**, 4023.
- Lewandowski, J. L. V. (1997b). *J. Phys. Soc. Japan* **66**, 3831.
- Lewandowski, J. L. V. (1997c). *Can. J. Phys.* **75**, 891.
- Lewandowski, J. L. V. (1998). *Plasma Phys. Contr. Fusion* **40**, 283.
- Liewer, P. C. (1985). *Nucl. Fusion* **25**, 543.
- Manheimer, W. D., and Lashmore-Davies, C. N. (1989). ‘MHD and Microinstabilities in Confined Plasma’ (Hilger: Bristol).
- Marchand, R., and Guzdar, P. N. (1982). *Phys. Fluids* **25**, 2037.
- Persson, M., and Lewandowski, J. L. V. (1997). *Plasma Phys. Contr. Fusion* **39**, 1941.
- Persson, M., Lewandowski, J. L. V., and Nordman, H. (1996). *Phys. Plasmas* **2**, 3440.
- Press, W. H., Flannery, B. P., Teukolsky, S. A., and Vetterling, W. T. (1983). ‘Numerical Recipes in Fortran’ (Cambridge University Press).
- Rosenbluth, M. N., and Sagdeev, R. Z. (1984). ‘Basic Plasma Physics’, Vol. 2 (Elsevier: Amsterdam).
- Schlitt, L. G., and Hendel, H. W. (1972). *Phys. Fluids* **15**, 1578.
- Tang, J. T., and Luhmann, N. C. (1976). *Phys. Fluids* **19**, 1935.
- Tang, W. M. (1978). *Nucl. Fusion* **18**, 1089.
- Tsai, S.-T., Perkins, F. W., and Stix, T. H. (1970). *Phys. Fluids* **13**, 2108.
- Utsumi, T., Ikeda, M., and Takamura, M. (1994). In ‘Architecture of the VPP300 Parallel Supercomputer’ (Ed. A. Urioshi), p. 478 (Naka: Tokyo).
- Waltz, R. E., and Boozer, A. H. (1993). *Phys. Fluids B* **5**, 2201.
- Ware, A. S., Diamond, P. H., Biglari, H., Carreras, B. A., Charton, L. A., Leboeuf, J. N., and Wootton, A. J. (1992). *Phys. Fluids B* **4**, 877.

## Appendix A: Numerical Equilibrium

In this Appendix, we discuss the numerical equilibrium used in the 3-field model (15)–(17) for collisional drift in stellarator geometry. The characteristics of the toroidal heliac H1-NF (Hamberger *et al.* 1990) are also briefly discussed.

The toroidal heliac H1-NF is a 3-field period machine. The coil set consists of a central ring coil linked by 36 smaller toroidal field coils, a set of vertical field coils, which are not topologically linked to the main coil set, and a smaller helical coil fitted closely to the central coil. The average major radius  $\bar{R}$  is 1 m. The magnetic field strength at the magnetic axis is 1 T and the aspect ratio is  $A \equiv \bar{a}/\bar{R} = 7.6$  ( $\bar{a}$  is the average minor radius). The equilibrium has been computed using the VMEC code (Hirshman and Whitson 1983; Hirshman and Meier 1985) with fixed boundary conditions, zero net toroidal current and

a volume-averaged  $\beta$  of 0.35% for a set of 100 magnetic surfaces. The VMEC code solves the following ideal MHD equations

$$\mathbf{J} \times \mathbf{B} = c\nabla p, \quad \mathbf{J} = \frac{c}{4\pi} \nabla \times \mathbf{B}, \quad \nabla \cdot \mathbf{B} = 0, \quad (\text{A1})$$

which are the radial force balance equation, Ampere's law and the divergence-free condition for  $\mathbf{B}$ , respectively. The VMEC equilibrium code outputs the curvilinear components of the magnetic field, the Jacobian of the transformation as well as the cylindrical components of a set of magnetic surfaces in terms of Fourier series. The position vector on a given magnetic surface is written in cylindrical coordinates,  $\mathbf{r} = R \cos \phi \hat{\mathbf{x}} + R \sin \phi \hat{\mathbf{y}} + Z \hat{\mathbf{z}}$ , where  $\phi$  is the usual azimuthal angle. Coordinates  $(R, Z, \phi)$  are written in Fourier series as follows (for a given magnetic surface,  $s = \text{const}$ ):

$$\begin{aligned} R &= \sum_{m=0}^M \sum_{n=-N}^{n=+N} R_{mn} \cos(\mu_{mn}), \\ Z &= \sum_{m=0}^M \sum_{n=-N}^{n=+N} Z_{mn} \sin(\mu_{mn}), \\ \phi &= \zeta - \frac{2\pi}{N_p} \sum_{m=0}^M \sum_{n=-N}^{n=+N} \tilde{\phi}_{mn} \sin(\mu_{mn}), \end{aligned} \quad (\text{A2})$$

where  $\mu_{mn} \equiv m\theta + N_p n\zeta$  and  $N_p$  is the number of field periods. For H1-NF, we have  $N_p = 3$ . In view of the complicated magnetic field structure of H1-NF, a large number of Fourier components in (A2) must be retained; in this paper, we have chosen  $M = 13$  and  $N = 27$ .

Using equations (A2) the covariant basis vectors

$$\mathbf{e}_s \equiv \frac{\partial \mathbf{r}}{\partial s}, \quad \mathbf{e}_\theta \equiv \frac{\partial \mathbf{r}}{\partial \theta}, \quad \mathbf{e}_\zeta \equiv \frac{\partial \mathbf{r}}{\partial \zeta}, \quad (\text{A3})$$

can be computed, followed by the contravariant basis vectors (D'haeseleer *et al.* 1983)

$$\nabla_s \equiv \frac{\mathbf{e}_\theta \times \mathbf{e}_\zeta}{\mathcal{J}}, \quad \nabla_\theta \equiv \frac{\mathbf{e}_\zeta \times \mathbf{e}_s}{\mathcal{J}}, \quad \nabla_\zeta \equiv \frac{\mathbf{e}_s \times \mathbf{e}_\theta}{\mathcal{J}}. \quad (\text{A4})$$

The Jacobian of the transformation,  $\mathcal{J}$ , can be calculated using the set of contravariant basis vectors:  $\mathcal{J} = [\nabla_s \cdot (\nabla_\theta \times \nabla_\zeta)]^{-1}$ ; or using the set of covariant basis vectors:  $\mathcal{J} = \mathbf{e}_s \cdot (\mathbf{e}_\theta \times \mathbf{e}_\zeta)$ . Using equations (A3) and (A4), any vector quantity can be written in term of the covariant basis vectors or the contravariant basis vectors.

## Appendix B: Geometrical Effects

In this Appendix, we derive all the geometrical quantities that enter the model equations (15)–(17). Special attention is given to the effect arising from a

nonzero  $\theta_k$ . The relevant geometrical quantities are  $\xi_\perp$  (normalised perpendicular wavevector),  $\nabla_\parallel$  (parallel gradient operator keeping the field line label  $\alpha$  and the radial coordinate  $s$  constant),  $S_{\perp 1}$  (curvature term) and  $S_{\perp 2}$  (diamagnetic term). In particular, we show that only  $\xi_\perp$  and  $S_{\perp 1}$  are affected by a nonzero  $\theta_k$ .

The magnitude of the normalised perpendicular wavevector is defined by  $\xi_\perp \equiv (\hat{e}_\perp \cdot \hat{e}_\perp)^{\frac{1}{2}}$ . Hence, we can write

$$\xi_\perp = \frac{\bar{a}}{q(s)} [g^{\alpha\alpha} + 2\dot{q}\theta_k g^{s\alpha} + (\dot{q}\theta_k)g^{ss}]^{\frac{1}{2}}, \quad (\text{B1})$$

where the metric elements are

$$g^{\alpha\alpha} \equiv \nabla\alpha \cdot \nabla\alpha = g^{s\zeta} - 2qg^{\theta\zeta} + q^2g^{\theta\theta} + \dot{q}\theta[\dot{q}\theta g^{ss} + 2qg^{s\theta} - 2g^{s\zeta}], \quad (\text{B2})$$

$$g^{s\alpha} \equiv \nabla s \cdot \nabla\alpha = g^{s\zeta} - qg^{s\theta} - \dot{q}\theta g^{ss}, \quad (\text{B3})$$

and where  $g^{ss} \equiv \nabla s \cdot \nabla s$ ,  $g^{s\theta} \equiv \nabla s \cdot \nabla\theta$ ,  $g^{s\zeta} \equiv \nabla s \cdot \nabla\zeta$ ,  $g^{\theta\theta} \equiv \nabla\theta \cdot \nabla\theta$ ,  $g^{\theta\zeta} \equiv \nabla\theta \cdot \nabla\zeta$  and  $g^{\zeta\zeta} \equiv \nabla\zeta \cdot \nabla\zeta$  can be calculated using the methods outlined in Appendix A. We note that the last three terms on the right-hand side of equation (B2) and the last term on the right-hand side of equation (B3) are responsible for the *secular* behaviour of the perpendicular wavevector for a configuration with a nonvanishing global magnetic shear ( $\dot{q} \neq 0$ ). We note that a nonzero  $\theta_k$  yields the appearance of new secular terms in the norm of the normalised perpendicular wavevector (B1).

We now determine the parallel gradient operator. In Boozer (1980, 1981) coordinates the covariant representation of the confining magnetic field is

$$\mathbf{B} = B_s \nabla s + B_\theta(s) \nabla\theta + B_\zeta(s) \nabla\zeta, \quad (\text{B4})$$

where  $B_\theta$  and  $B_\zeta$  are flux surface quantities which are respectively related to the toroidal and poloidal currents flowing in the plasma. Taking the scalar product of equation (B4) with the contravariant form (1), we note that  $\mathcal{J}B^2$  is a flux surface quantity. This flux surface quantity

$$F(s) \equiv \mathcal{J}B^2 \quad (\text{B5})$$

can be used to simplify analytical formulation of equilibrium quantities. We now proceed with the parallel gradient operator. Introducing  $\bar{\eta} \equiv \theta B_\theta(s) + \zeta B_\zeta(s)$  and  $B_s^* \equiv B_s - \theta \dot{B}_\theta - \zeta \dot{B}_\zeta$  (where a dot denotes  $d/ds$ ), the magnetic field can be written in the set of intermediate coordinates  $(s, \alpha, \bar{\eta})$ , which yields

$$\mathbf{B} = B_s^* \nabla s + \nabla \bar{\eta}. \quad (\text{B6})$$

Using equation (B6), the parallel gradient operator, keeping  $s$  (on a given magnetic surface) and  $\alpha$  (on a given magnetic field line) constant, can now be written as

$$\begin{aligned}
\nabla_{\parallel} &= \left( \hat{\mathbf{e}}_{\parallel} \cdot \nabla s \frac{\partial}{\partial s} + \hat{\mathbf{e}}_{\parallel} \cdot \nabla \alpha \frac{\partial}{\partial \alpha} + \hat{\mathbf{e}}_{\parallel} \cdot \nabla \bar{\eta} \frac{\partial}{\partial \bar{\eta}} \right)_{s,\alpha} \\
&= \left( \frac{\mathbf{B} \cdot \nabla \bar{\eta}}{B} \right)_{s,\alpha} \frac{\partial}{\partial \bar{\eta}} \\
&= B \frac{\partial}{\partial \bar{\eta}}, \tag{B7}
\end{aligned}$$

where we have made use of equation (B6). Clearly the coordinate  $\bar{\eta}$  is related to the length along the magnetic field line,  $dx_{\parallel} = d\bar{\eta}/B$  ( $x_{\parallel}$  is the length along the magnetic field line). On a given magnetic field,  $d\alpha = 0$ , we may write  $d\theta = d\zeta/q(s)$  and the parallel gradient operator becomes

$$\nabla_{\parallel} = \frac{\xi_{\parallel}(\zeta)}{\bar{R}} \frac{\partial}{\partial \zeta}, \tag{B8}$$

where  $\xi_{\parallel} \equiv 1/\mathcal{J}_{\star} B_{\star}$  is a function, defined along the extended toroidal angle, of the order of unity. Here  $\mathcal{J}_{\star} \equiv 2\mathcal{J}/\bar{a}^2 \bar{R} \sim 1$  is the normalised Jacobian.

We now derive the expressions for the cross-field ‘source terms’  $S_{\perp 1}$  (curvature term) and  $S_{\perp 2}$  (diamagnetic term). Recalling the definition of the unit normal vector  $\hat{\mathbf{n}} \equiv \nabla s / (\nabla s \cdot \nabla s)^{\frac{1}{2}}$ , we write the diamagnetic term as

$$\begin{aligned}
S_{\perp 2} &= \frac{\bar{a} \sqrt{g^{ss}}}{B_{\star}} \hat{\mathbf{e}}_{\parallel} \cdot (\hat{\mathbf{n}} \times \hat{\mathbf{e}}_{\perp}) \\
&= \frac{\bar{a}^2 \sqrt{g^{ss}}}{q B_{\star}} \hat{\mathbf{e}}_{\parallel} \cdot \left[ \frac{\nabla s}{\sqrt{g^{ss}}} \times (\nabla \alpha + \dot{q} \theta_k \nabla s) \right] \\
&= \frac{\bar{a}^2 \dot{\psi}}{q B B_{\star}} (\nabla \alpha \times \nabla s) \cdot [\nabla s \times \nabla \alpha + \dot{q} \theta_k \nabla s \times \nabla s] \\
&= \frac{\bar{a}^2 \dot{\psi} B_0}{q B^2} (\nabla \alpha \times \nabla s) \cdot (\nabla s \times \nabla \alpha) \\
&= -\frac{\bar{a}^2 B_0}{q \dot{\psi}} = -2, \tag{B9}
\end{aligned}$$

where we have used the definition of the enclosed toroidal flux  $\Psi(s) = B_0 \pi \bar{a}^2 s$ , from which one easily obtains  $\dot{\psi} = B_0 \bar{a}^2 / 2q$ . As apparent from equation (B9),  $S_{\perp 2}$  is independent of  $\theta_k$ . We would like to point out that the result  $S_{\perp 2} = \text{const}$  applies to both axi-symmetric plasmas (e.g. tokamak plasmas) and asymmetric plasmas (e.g. stellarator plasmas).

We now calculate the curvature term,  $S_{\perp 1}$ . We note that the magnetic field curvature can be written in the form  $\boldsymbol{\kappa} = \kappa_N \hat{\mathbf{n}} + \kappa_G \hat{\mathbf{b}}$ , where  $\hat{\mathbf{b}} \equiv \hat{\mathbf{e}}_{\parallel} \times \hat{\mathbf{n}}$  is the unit binormal vector (D’haeseleer *et al.* 1983). Here  $\kappa_N \equiv \hat{\mathbf{n}} \cdot \boldsymbol{\kappa}$  and  $\kappa_G \equiv \hat{\mathbf{b}} \cdot \boldsymbol{\kappa}$  are the normal and geodesic components of the magnetic field curvature, respectively. In the low- $\beta$  approximation, the magnetic field curvature can be written as  $\boldsymbol{\kappa} \simeq (\hat{\mathbf{n}}\hat{\mathbf{n}} + \hat{\mathbf{b}}\hat{\mathbf{b}}) \cdot \nabla B / B$ . Since the unit vectors  $\hat{\mathbf{e}}_{\parallel}$  and  $\hat{\mathbf{n}}$  are known, we can

calculate the unit binormal  $\widehat{\mathbf{b}} = \widehat{\mathbf{e}}_{\parallel} \times \widehat{\mathbf{n}}$  (see also Appendix A). Then, the *perpendicular* tensor  $\widehat{\mathbf{n}}\widehat{\mathbf{n}} + \widehat{\mathbf{b}}\widehat{\mathbf{b}}$  is known. To calculate the  $\nabla B$  term, we use the flux surface quantity (B5) to obtain

$$\frac{\nabla B}{B} = \frac{1}{2} \left( \frac{\dot{F}}{F} - \frac{1}{\mathcal{J}} \frac{\partial \mathcal{J}}{\partial s} \right) \nabla s - \frac{1}{2\mathcal{J}} \frac{\partial \mathcal{J}}{\partial \theta} \nabla \theta - \frac{1}{2\mathcal{J}} \frac{\partial \mathcal{J}}{\partial \zeta} \nabla \zeta. \quad (\text{B10})$$

Using equation (B10) and noting that

$$\begin{aligned} \widehat{\mathbf{e}}_{\parallel} \times \widehat{\mathbf{e}} &= \frac{\dot{\psi}}{B} (\nabla \alpha \times \nabla s) \times \frac{\bar{a}}{q} (\nabla \alpha + \dot{q}\theta_k \nabla s) \\ &= \frac{\bar{a}\dot{\psi}}{qB} [(\nabla \alpha \times \nabla s) \times \nabla \alpha + \dot{q}\theta_k \nabla s \times (\nabla s \times \nabla \alpha)] \\ &= \frac{\bar{a}\dot{\psi}}{qB} [(g^{\alpha\alpha} + \dot{q}\theta_k g^{s\alpha}) \nabla s - (g^{s\alpha} + \dot{q}\theta_k g^{ss}) \nabla \alpha], \end{aligned} \quad (\text{B11})$$

we may write the curvature term as

$$\begin{aligned} S_{\perp 1} &= \frac{L_n \bar{a}^3}{2(qB_*)^2} \left[ \left( \frac{1}{F} \frac{dF}{ds} - \frac{1}{\mathcal{J}} \frac{\partial \mathcal{J}}{\partial s} \right) [g^{ss}(g^{\alpha\alpha} + \dot{q}\theta_k g^{s\alpha}) - g^{s\alpha}(g^{s\alpha} + \dot{q}\theta_k g^{ss})] \right. \\ &\quad - \frac{1}{\mathcal{J}} \frac{\partial \mathcal{J}}{\partial \theta} [g^{s\theta}(g^{\alpha\alpha} + \dot{q}\theta_k g^{s\alpha}) - g^{\theta\alpha}(g^{s\alpha} + \dot{q}\theta_k g^{ss})] \\ &\quad \left. - \frac{1}{\mathcal{J}} \frac{\partial \mathcal{J}}{\partial \zeta} [g^{s\zeta}(g^{\alpha\alpha} + \dot{q}\theta_k g^{s\alpha}) - g^{\zeta\alpha}(g^{s\alpha} + \dot{q}\theta_k g^{ss})] \right]. \end{aligned} \quad (\text{B12})$$

All quantities on the right-hand side of equation (B12) are evaluated along the extended toroidal angle. We note that the inclusion of finite  $\theta_k$  leads to the appearance of many new secular terms. If we consider the limit  $\theta_k \rightarrow 0$ , we recover the previously determined results (Lewandowski 1997a, 1997b). Although it is not apparent in equation (B12), the curvature effects of the magnetic surface are actually contained in the partial derivatives of the Jacobian. For example, the explicit form for  $\partial \mathcal{J} / \partial \zeta$  in equation (B12) is given by

$$\frac{\partial \mathcal{J}}{\partial \zeta} = \mathbf{G}_{s\zeta} \cdot (\mathbf{e}_\theta \times \mathbf{e}_\zeta) + \mathbf{e}_s \cdot (\mathbf{G}_{\theta\zeta} \times \mathbf{e}_\zeta + \mathbf{e}_\theta \times \mathbf{G}_{\zeta\zeta}), \quad (\text{B13})$$

where  $\mathbf{G}_{ij} \equiv \partial^2 \mathbf{r} / \partial i \partial j$ , for  $(i, j) = \{s, \theta, \zeta\}$ , is the *curvature* of the local position vector  $\mathbf{r}$ . All of the elements  $\mathbf{G}_{ij}$  can be easily calculated using the results of Appendix A.